On the Optimal Detection of an Underwater Intruder in a Channel Using Unmanned Underwater Vehicles

Hoam Chung,[1] Elijah Polak,[2] Johannes O. Royset,[3] Shankar Sastry[2]

[1] *Department of Mechanical and Aerospace Engineering, Monash University, Clayton, Australia*

[2] *Department of Electrical Engineering and Computer Sciences, University of California, Berkeley*

[3] *Department of Operations Research, Naval Postgraduate School, Monterey, California*

Received 15 July 2010; revised 13 September 2011; accepted 25 September 2011
DOI 10.1002/nav.20487
Published online 24 October 2011 in Wiley Online Library (wileyonlinelibrary.com).

Abstract: Given a number of patrollers that are required to detect an intruder in a channel, the channel patrol problem consists of determining the periodic trajectories that the patrollers must trace out so as to maximized the probability of detection of the intruder. We formulate this problem as an optimal control problem. We assume that the patrollers' sensors are imperfect and that their motions are subject to turn-rate constraints, and that the intruder travels straight down a channel with constant speed. Using discretization of time and space, we approximate the optimal control problem with a large-scale nonlinear programming problem which we solve to obtain an approximately stationary solution and a corresponding optimized trajectory for each patroller. In numerical tests for one, two, and three underwater patrollers, an underwater intruder, different trajectory constraints, several intruder speeds and other specific parameter choices, we obtain new insight—not easily obtained using simply geometric calculations—into efficient patrol trajectory design under certain conditions for multiple patrollers in a narrow channel where interaction between the patrollers is unavoidable due to their limited turn rate. © 2011 Wiley Periodicals, Inc. Naval Research Logistics 58: 804–820, 2011

Keywords: search theory; military operations research; optimal control model

1. INTRODUCTION

This article deals with the optimal detection of an underwater intruder in a channel using one or more unmanned underwater vehicles (UUVs). In particular, it establishes optimal periodic patrol trajectories for the UUVs, which we refer to as patrollers, that maximize the probability of detection of an underwater intruder traveling straight down a channel at constant speed. While we focus on an underwater intruder and patrollers, our general approach may also be applicable in the case of other types of vehicles.

This problem is a multipatroller extension of the classical "channel patrol problem" (also called the barrier patrol problem); see, e.g., Section 1.3 of [16] and Chapter 9 of [15]. The channel patrol problem for a single patroller was formulated by Koopman [8] during World War II and arises in naval operations where the channel may represent a relatively narrow body of water such as a strait or port entrance through which enemy vessels and submarines as well as smugglers and terrorists may attempt to pass. The channel patrol problem may also arise in anti-submarine warfare in an operating area around a carrier or naval expeditionary strike group [13] and then typically with multiple patrollers. With the proliferation of small diesel submarines and the advent of UUVs and self-propelled semi-submersibles the channel patrol problem has acquired new importance, since these vessels are difficult to detect.[1] The need to consider multiple patrollers is apparent, especially in view of the development of small UUVs that may be used to guard channels.

The early studies by Koopman [8] and by Washburn [17] focus on the determination of the probability of intruder detection for a single patrol trajectory consisting of piecewise

Correspondence to: J.O. Royset (joroyset@nps.edu)

[1] Quoting from Daily Mail Online, November 11th, 2007, "American military chiefs have been left dumbstruck by an undetected Chinese submarine popping up at the heart of a recent Pacific exercise and close to the vast U.S.S. Kitty Hawk - a 1000 ft super carrier with 4500 personnel on board. By the time it surfaced the 160 ft Song Class diesel-electric attack submarine is understood to have sailed within viable range for launching torpedoes or missiles at the carrier," by Matthew Hickley.

linear segments; see also Chapter 9 of [15]. (We refer the reader to [1] for a broad review of other problems in search theory). This approach results in simple formulae for the probability of detection and provides insight into the effectiveness of "back-and-forth" versus "bow-tie" trajectories for various patroller and intruder speeds. In reality, a vessel cannot carry out a perfect back-and-forth patrol trajectory as it is unable to turn around instantaneously at the end of each channel crossing. These early studies ignore the limited turn-radius of the patroller or use coarse approximations. Moreover, they focus on a single patroller with the assumption that the case of multiple patrollers can be solved by dividing the channel into subchannels, with one patroller assigned to each subchannel. This policy may become problematic when there are many patrollers in a narrow channel. In that case, the limited turn radius of a patroller may force it to deviate greatly from the assigned, say, back-and-forth trajectory.

In this study, we consider one or more patrollers, account for turn-radius limits and imperfect sensors, and model the motion of the patrollers using ordinary differential equations. This formulation leads to an optimal control problem with solution trajectories that are executable by UUVs. Optimal control formulations of general search problems are found in [4] with later generalizations in [11]; see also references therein. However, these studies deal with the general situation where the intruder moves according to some diffusion process. We take advantage of the special structure of the channel patrol problem and derive significantly simpler expressions, which allow us to carry out a comprehensive numerical investigation of one, two, and three patrollers.

In Section 2, we derive a formula for the detection probability, in Section 3 we present the optimal control formulation of the channel patrol problem, and in Section 4 we discuss a discretization scheme for this optimal control problem. Numerical results are found in Section 5, which is followed by our concluding remarks in Section 6. An Appendix generalizes the formulation and discretization scheme of Sections 3 and 4 from two-dimensional to three-dimensional patrollers.

2. DETECTION PROBABILITY

We consider a scenario of patrolling a channel similar to the one in [17]: patrollers search a channel of width L looking for a single intruder which is moving straight down the channel with constant speed v_I (see Fig. 1). The intruder is unaware of the patrollers, makes no attempt to evade them, and simply progresses straight down the channel with an unknown (to the patrollers) distance to the sides of the channel. This assumption is reasonable when examining the situation before the intruder detects the patrollers and vice versa, which is the focus of this paper. During this "detection phase" neither side has much information about each other. The patrollers' assumption about a straight intruder trajectory is reasonable for at least two reasons: (i) submarines generate additional noise and become more vulnerable to detection when turning and (ii) the shortest distance to "the end of the channel" is along a straight line. Of course, after detection (one-sided or mutual), a pursuit-evasion game starts. We do not consider that phase, which requires new models (see, for example, Refs. 3, 9, and 14) and is better postponed to a follow-up paper.

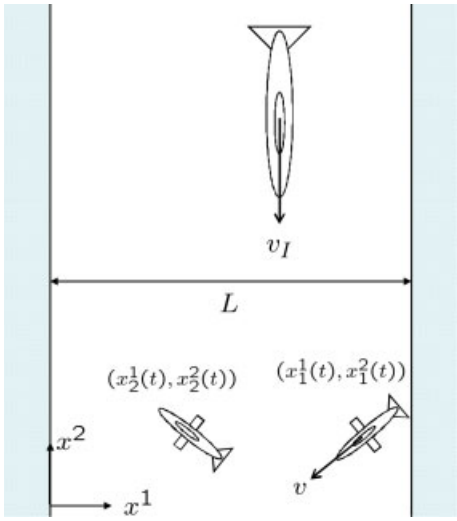

Figure 1. Two patrollers (bottom) try to detect an intruder (top) in a channel. [Color figure can be viewed in the online issue, which is available at wileyonlinelibrary.com.]

We assume that the probability of detection, of the intruder by a patroller, depends on the positions of the patroller and the intruder, the quality of the patroller's sensor, and on the time allowed for observation. We also could easily let the probability of detection depend on the speeds of the intruder and patrollers, but ignore that possibility here to avoid complicated detection models. (We do explore one effect of variable intruder speed in Section 5).

Suppose that there are q patrollers looking independently for the intruder and that $\hat{x}_k(t) \triangleq (x_k^1(t), x_k^2(t)) \in \mathbb{R}^2$ is the position of the k-th patroller at time t, $k = 1, 2, \ldots, q$, see Fig. 1 for the case with $q = 2$. We use superscripts to denote components of a vector. We here assume that the patrollers and the intruder do not vary their depth, which is the case, for example, in a shallow channel where maneuverability in the depth-dimension may be limited. In other cases, depth variations may be significant and should be accounted for in the model formulation. For simplicity of exposition, we consider the two-dimensional case in the main part of the paper, but include an appendix summarizing the three-dimensional model and discretization scheme.

We derive the expression for the probability of detection in two steps. First, we derive the detection probability for a

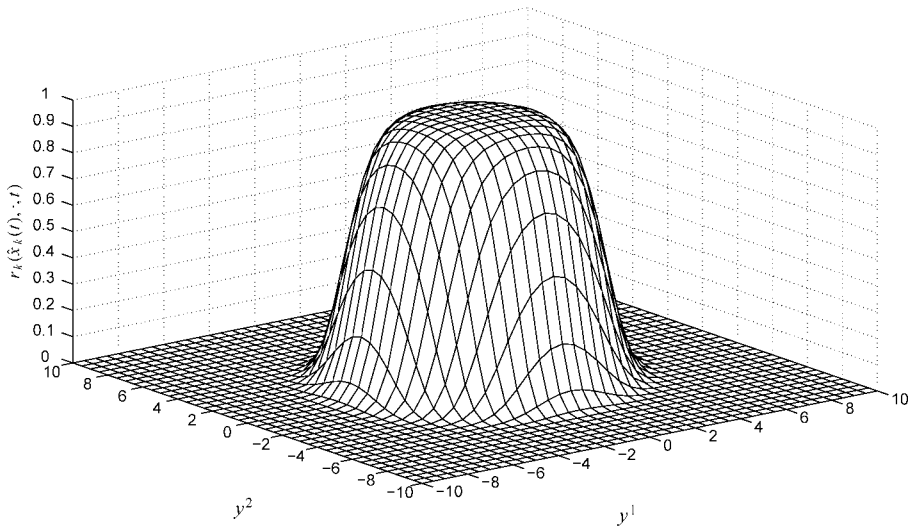

Figure 2. Detection rate function based on Poisson Scan Model (1).

stationary intruder. Second, we extend that expression to the situation at hand with a moving intruder in a channel. Hence, temporarily assume that the intruder is stationary and located at $y \in \mathbb{R}^2$. Again, an extension of the following formulation to three dimensions is trivial. Let $r_k(\hat{x}_k(t), y, t) \geq 0$, $k = 1, 2, \ldots, q$, denote the detection rate at time t for the k-th patroller at $\hat{x}_k(t)$ when the intruder is located at y. The detection rates reflect the qualities of the patrollers' sensors as described in more details below and are defined so that the probability that the k-th patroller detects the intruder during a small time interval $[t, t + \Delta t)$ is $r_k(\hat{x}_k(t), y, t)\Delta t$. For theoretical and computational reasons, $r_k(\cdot, \cdot, \cdot)$, $k = 1, 2, \ldots, q$, must be smooth, but can otherwise take any form to reflect a variety of sensors.

We focus on patrollers that are UUVs and intruders that are diesel-electric submarines, and assume that the patrollers' sensors are sonars. A large class of sensor models can be handled by our framework or minor adjustment thereof, but to avoid classified data we adopt the relative simple Poisson Scan Model (see, e.g., [16] p. 3-1) to illustrate our approach. Hence, for the k-th patroller, we set

$$r_k(\hat{x}_k(t), y, t) = \lambda \Phi[\{F_k - \rho(\hat{x}_k(t), y)\}/\sigma], \qquad (1)$$

where $\Phi(\cdot)$ is the standard normal cumulative distribution function, λ is the scan opportunity rate, F_k is the "figure of merit" (a sonar characteristic), σ reflects the variability in the "signal excess," and $\rho(\hat{x}_k(t), y)$ is the propagation loss, which depends on the distance between the patroller and the intruder, see, e.g, Figure 4.5 on page 93 in [15]. All these quantities may be time dependent. The typical shape of $r_k(\hat{x}_k(t), \cdot, t)$ is shown in Fig. 2, where $\hat{x}_k(t) = (0, 0)$ and $\rho(\hat{x}_k(t), y) = a\|\hat{x}_k(t) - y\|^2 + b$, with $\lambda = 1$, $F_k = 70$, $\sigma = 5$, $a = 0.5$, and $b = 60$. We now define the probability that the k-th patroller does not detect the intruder during some time interval $[0, T]$ in terms of the detection rate.

Given a trajectory $\{\hat{x}_k(t), 0 \leq t \leq T\}$ and an intruder at y, we denote the probability that the k-th patroller does not detect the intruder during $[0, t]$, $t \in [0, T]$, by $p_k(y, t)$. Assuming that events of detection in non-overlapping time intervals are all independent, we find that this probability can be computed recursively by solving the difference equation

$$p_k(y, t + \Delta t) = p_k(y, t)(1 - r_k(\hat{x}_k(t), y, t)\Delta t), \quad p_k(y, 0) = 1, \qquad (2)$$

or, as Δt tends to zero, by solving the parameterized differential equation

$$\frac{dp_k(y, t)}{dt} = -p_k(y, t) r_k(\hat{x}_k(t), y, t), \quad p_k(y, 0) = 1, \qquad (3)$$

with solution

$$p_k(y, t) = \exp(-\eta_k(y, t)), \qquad (4)$$

where

$$\eta_k(y, t) = \int_0^t r_k(\hat{x}_k(s), y, s) ds. \qquad (5)$$

The above derivation follows from standard arguments for Poisson processes and $\eta_k(y, t)$ is the mean value of the random number of detections at y, up to time t, by the k-th patroller, when that number is given by a Poisson law.

Now, let $\phi : \mathbb{R}^2 \to \mathbb{R}$ be the probability density function of the location of the (stationary) intruder at time 0, i.e., for

any $B \subset \mathbb{R}^2$, $\int_B \phi(y)dy$ is the probability that the intruder is located in the area B at time 0. This information may be provided by exogenous intelligence sources and reflects the patrollers knowledge about the intruder before the start of the patrols. Then, the probability that the k-th patroller fails to detect a stationary intruder during the time period $[0, T]$ is given by

$$\int_{y\in\mathbb{R}^2} p_k(y, T)\phi(y)dy \tag{6}$$

$$= \int_{y\in\mathbb{R}^2} \exp\left(-\int_0^T r_k(\hat{x}_k(t), y, t)dt\right)\phi(y)dy. \tag{7}$$

As it gives the probability that the k-th patroller does not detect the intruder during $[0, t]$, the function $p_k(\cdot, t)$ reflects the patroller's knowledge about the intruder's location at time t and can therefore be considered to be "information states" or "belief states" that augment the "physical state" $\hat{x}_k(t)$, $k = 1, 2, \ldots, q$.

The extension from a stationary intruder, as assumed above, to an intruder that moves straight down a channel at constant speed, see Fig. 1, is accomplished by a linear transformation as described next.

As in [17], we fix the position of the intruder on a tape moving down the channel at the speed of the intruder, v_I. Hence, the intruder is stationary relative to the tape and the formulae derived above are applicable. We only need to measure the patroller's location relative to the tape. In this framework, the probability of detection relates to the ratio of the rate at which the patroller examines new area on the tape to the rate at which new tape area appears.

To utilize this approach, let $\hat{z}_k(t) \triangleq (z_k^1(t), z_k^2(t))$ be the position vector of the k-th patroller at time t relative to the tape. Then we have that for all $k = 1, 2, \ldots, q$,

$$\begin{aligned} z_k^1(t) &= x_k^1(t) \\ z_k^2(t) &= x_k^2(t) + v_I t. \end{aligned} \tag{8}$$

We refer to $\hat{x}_k(t)$ and $\hat{z}_k(t)$ as the absolute and relative positions of the k-th patroller at time t, respectively. We will use y for both the absolute and relative positions of the intruder as the meaning is clear from the context.

Since the channel has width L, it suffices to consider relative intruder position $y \in A(T) \triangleq [0, L] \times [0, v_I T]$ for patrols of duration T time units. Hence, it follows from (7) that given a trajectory $\{\hat{z}_k(t), 0 \le t \le T\}$, the probability that the k-th patroller does not detect the intruder during time period $[0, T]$ is

$$P_k \triangleq \int_{y\in A(T)} \exp\left(-\int_0^T r_k(\hat{z}_k(t), y, t)dt\right)\phi(y)dy, \tag{9}$$

where the probability density function of the relative position of the intruder takes the specific form $\phi(y) = \phi^1(y^1)/(v_I T)$, with $\phi^1(\cdot)$ being the probability density function of the intruder's y^1-position (i.e., the intruder's horizontal position in Fig. 1). For example, if the patrollers have no prior knowledge of the y^1-position of the intruder, then one can assume a uniform distribution across the channel, i.e., $\phi^1(y^1) = 1/L$ for all $y^1 \in [0, L]$. Note that we abuse the notation $r_k(\cdot, \cdot, \cdot)$ slightly, by using it to represent the detection rate function both in the absolute and in the relative positions.

We assume that the patrollers make independent detection attempts and hence it follows from (4) and (5) that the conditional probability that no patroller detects the intruder given a specific relative intruder position y is simply the product

$$\begin{aligned} &\prod_{k=1}^{q} \exp\left(-\int_0^T r_k(\hat{z}_k(t), y, t)dt\right) \\ &\quad = \exp\left(-\sum_{k=1}^{q}\int_0^T r_k(\hat{z}_k(t), y, t)dt\right) \\ &\quad = \exp\left(-\int_0^T \sum_{k=1}^{q} r_k(\hat{z}_k(t), y, t)dt\right). \end{aligned} \tag{10}$$

Consequently, the probability that no patroller detects the intruder during $[0, T]$ takes the form

$$P \triangleq \int_{y\in A(T)} \exp\left(-\int_0^T \sum_{k=1}^{q} r_k(\hat{z}_k(t), y, t)dt\right)\phi(y)dy. \tag{11}$$

We use this expression in an optimal control problem for determining patrol trajectories as discussed next.

3. OPTIMAL CONTROL PROBLEM

Our objective is to find optimal closed trajectories for multiple patrollers that maximize the probability of detection of the intruder. In contrast to [17], we consider multiple patrollers whose turn radius is constrained by their dynamics, in differential equation form, and available control action. Thus we assume that the positions of the patrollers are states of a differential equation. Specifically, we assume that the kinematic equations of all the patrollers are the same and are of the form

$$\frac{dx_k(t)}{dt} = f(x_k(t), u_k(t)), \quad x_k(0) = \xi_k, \tag{12}$$

where the state $x_k(t) \in \mathbb{R}^{n_x}$, the control $u_k(t) \in \mathbb{R}^{n_u}$, $f : \mathbb{R}^{n_x} \times \mathbb{R}^{n_u} \to \mathbb{R}^{n_x}$ is locally Lipschitz continuous, and ξ_k is the initial condition of patroller k. We assume that the first two components of the state, $(x_k^1(t), x_k^2(t))$, represent the absolute location of the k-th patroller. Hence, $x_k(t) = (\hat{x}_k(t)', x_k^3(t), x_k^4(t), \ldots, x_k^{n_x}(t))'$, where prime denotes the

transpose of a vector. The assumption that all patrollers are governed by the same kinematic equation is easily relaxed, but requires further notation and is therefore avoided here.

Next, referring to (8), let $e_2 \triangleq (0,1,0,\ldots,0) \in \mathbb{R}^{n_x}$, and let $z_k(t) \triangleq x_k(t) + v_I t e_2$. Hence, $z_k(t) = (\hat{z}_k(t)', x_k^3(t), x_k^4(t), \ldots, x_k^{n_x}(t))'$. We refer to $x_k(t)$ and $z_k(t)$ as absolute and relative states for the k-th patroller, respectively. Then we find that the k-th patroller's dynamics in the relative state become

$$\frac{dz_k(t)}{dt} = \tilde{f}(z_k(t), u_k(t)), \quad z_k(0) = \xi_k, \tag{13a}$$

where

$$\tilde{f}(z_k(t), u_k(t)) \triangleq f(z_k(t) - v_I t e_2, u_k(t)) + v_I e_2. \tag{13b}$$

We let the patrol duration T be a decision variable. Hence, we introduce the time transformation $t = Ts$ to enable us to define the channel patrol problem on the fixed time interval $[0,1]$. For simplicity of notation, we use the same notation for states and controls defined on $[0,T]$ as on the normalized time interval $[0,1]$. The meaning should be clear from the context. We now obtain the time-normalized kinematic equations

$$\frac{dz_k(s)}{ds} = T\tilde{f}(z_k(s), u_k(s)), \quad z_k(0) = \xi_k. \tag{14}$$

We denote the solution of (14) by $z_k(\cdot; T, u_k, \xi_k)$, as it clearly depends on the control input $\{u_k(s), s \in [0,1]\}$, the time horizon T, and the initial condition ξ_k. As the relative location $\hat{z}_k(t)$ of the k-th patroller is given by the first two components of $z_k(\cdot; T, u_k, \xi_k)$ evaluated at t/T, it also depends on $\{u_k(s), s \in [0,1]\}$, T, and ξ_k. Moreover, the probability P that no patroller detects the intruder during the interval $[0,T]$ (see (11)) is a function of T and the relative locations $\{\hat{z}_k(t), t \in [0,T]\}$, $k = 1,2,\ldots,q$. Consequently, P depends on T, $\{u_k(s), s \in [0,1]\}$ and ξ_k, $k = 1,2,\ldots,q$, and to emphasize this dependence we write $P(T,u,\xi)$ instead of P, where $u = (u_1, u_2, \ldots, u_q)$ and $\xi = (\xi_1, \xi_2, \ldots, \xi_q)$.

The optimal periodic patrol problem (OPPP) consists of maximizing the probability of detecting the intruder during the time interval $[0,T]$, i.e., $1 - P(T,u,\xi)$, by choosing the best values of T, u, and ξ. This leads to the following optimal control problem formulation:

$$\begin{aligned}
\textbf{OPPP}: \quad & \max\{1 - P(T,u,\xi)\} && (15a)\\
& \text{s.t. } z_k(1;T,u_k,\xi_k) = g(\xi_k), k = 1,2,\ldots,q, && (15b)\\
& z_k(s;T,u_k,\xi_k) \le z_k^{\max}(s;T), k = 1,2,\ldots,q, s \in [0,1], && (15c)\\
& z_k(s;T,u_k,\xi_k) \ge z_k^{\min}(s;T), k = 1,2,\ldots,q, s \in [0,1], && (15d)\\
& T \in [T^{\min}, T^{\max}], && (15e)\\
& u \in \mathbf{U}, && (15f)\\
& \xi \in \mathbf{X}, && (15g)
\end{aligned}$$

where $g : \mathbb{R}^{n_x} \to \mathbb{R}^{n_x}$ is a function that describes the end-state constraints, $z_k^{\max}(s;\cdot) : \mathbb{R} \to \mathbb{R}^{n_x}$ and $z_k^{\min}(s;\cdot) : \mathbb{R} \to \mathbb{R}^{n_x}$ are upper and lower bounds on the state trajectories at scaled time s, respectively, $T^{\min}$ and $T^{\max}$ are the minimum and maximum durations of a patrol, respectively, $\mathbf{U}$ is the set of admissible controls, and $\mathbf{X} \subset \mathbb{R}^{n_x} \times \cdots \times \mathbb{R}^{n_x}$ is the set of admissible initial conditions. We note that the inequalities in (15c) and (15d) are componentwise. We assume that $\mathbf{U}$ is a convex subset of the q-dimensional Cartesian product $L_{\infty,2}^{n_u}[0,1] \times \cdots \times L_{\infty,2}^{n_u}[0,1]$, where $L_{\infty,2}^{n_u}[0,1]$ denotes the pre-Hilbert space whose elements are functions from $[0,1]$ to $\mathbb{R}^{n_u}$, which are in $L_{\infty}^{n_u}[0,1]$, i.e, are sup-norm bounded, with inner product $\langle u_1, u_2\rangle_2 \triangleq \int_0^1 \langle u_1(t), u_2(t)\rangle dt$ and norm $\|\cdot\|_2$ defined by $\|u\|_2 = \langle u, u\rangle_2^{1/2}$.[2] Specifically, we let

$$\begin{aligned}
\mathbf{U} \triangleq \{u = (u_1, u_2, \ldots, u_q) | u_k \in L_{\infty,2}^{n_u}[0,1], u_k^{\min} \le u_k(s) \\
\le u_k^{\max}, \forall s \in [0,1], k = 1,2,\ldots,q\}
\end{aligned} \tag{16}$$

[2] The reason for using this "hybrid" space is that our cost and constraint functions are differentiable on $L_{\infty,2}^{nu}[0,1]$, but they are not necessarily differentiable on the well-know space $L_2^{nu}[0,1]$ of Lebesgue square-integrable functions with the same scalar product and norm; see Section 5.6 in [12].

where $u_k^{\min}$ and $u_k^{\max}$ are the minimum and maximum control input at any point in time for the k-th patroller.

We use the constraints (15b) to ensure that the patrollers' trajectories are closed. The constraints (15c) and (15d) are set up to contain the trajectories of the patrollers to be within a time-varying box. The constraint (15e) limits the duration of a patrol. The constraints (15f) and (15g) ensure that the control input and initial conditions satisfy specific constraints. We note that the dynamics (14) are implicitly accounted for through the definition of $P(T,u,\xi)$ and $z_k(\cdot;u_k,T,\xi_k)$, $k=1,2,\ldots,q$.

We replace the "running cost" $\exp(-\int_0^T \sum_{k=1}^q r_k(\hat{z}_k(t), y, t)dt)$ in (11) with an "end cost" using an auxiliary information state $p(y,s)$ to facilitate the evaluation of this integral by the same numerical integration technique used to solve the dynamic equations (14). For any $y \in \mathbb{R}^2$, let $p(y,s)$ be the solution of the parameterized differential equation

$$\frac{dp(y,s)}{ds} = -Tp(y,s)\sum_{k=1}^{q} r_k(\hat{z}_k(s), y, Ts), \quad p(y,0)=1. \tag{17}$$

In view of (3), $p(y,s)$ is the probability that no patroller has detected the intruder during the time interval $[0, Ts]$ given that the intruder is located at y. It generalizes the information state $p_k(y,t)$ to the case of multiple patrollers, relative locations, and scaled time.

In this notation,

$$P(T,u,\xi) = \int_{y\in A} p(y,1)\phi(y)dy, \tag{18}$$

where $p(y,1)$ is given by (17) and computed using T, u, and ξ, and $A \triangleq [0,L]\times[0,v_I]$. Note that similarly to the change from the time interval $[0,T]$ to the scaled time interval $[0,1]$, the area $A(T)=[0,L]\times[0,v_IT]$ is replaced by the scaled area A.

The numerical solution of **OPPP** requires the discretization of the time interval $[0,1]$ and of the area A, as we describe in the next section.

4. DISCRETIZATION

We consider the time and space discretizations in turn. First, we deal with the discretization of the rectangular area A, using a N_1 by N_2 grid defined by

$$y_i^1 = i\Delta_1 \text{ and } y_j^2 = j\Delta_2, \tag{19}$$

where $\Delta_1 = L/N_1$, $\Delta_2 = v_I/N_2$, $i=0,1,\ldots,N_1$, and $j=0,1,\ldots,N_2$. We also define center points of the grid by

$$y_c^{(i,j)} = \begin{bmatrix} y_i^1 - \Delta_1/2 \\ y_j^2 - \Delta_2/2 \end{bmatrix}, \tag{20}$$

for $i=1,2,\ldots,N_1$ and $j=1,2,\ldots,N_2$.

Let $p_{ij}(s) \triangleq p(y_c^{(i,j)}, s)$. Then, for the center points of this grid, (17) becomes

$$\frac{dp_{ij}(s)}{ds} = -Tp_{ij}(s)\sum_{k=1}^{q} r_k\big(\hat{z}_k(s), y_c^{(i,j)}, Ts\big),\ p_{ij}(0)=1. \tag{21}$$

This discretization approach works with *any* spatial discretization scheme. For example, if the given problem is to find a patrolling trajectory inside a closed area with an arbitrary shape, one can use a triangular mesh grid.

Second, we consider discretization of the dynamics in time. We follow the procedure described in [12] and use Euler's method with time step $\Delta = 1/N$, N a positive integer, to obtain the discretized dynamics of (14) and (21):

$$z_k((l+1)\Delta) - z_k(l\Delta) = \Delta T\,\tilde{f}(z_k(l\Delta), u_k(l\Delta)), z_k(0)=\xi_k, \tag{22a}$$

for $k=1,2,\ldots,q$ and

$$p_{ij}((l+1)\Delta) - p_{ij}(l\Delta) = -\Delta T p_{ij}(l\Delta)\sum_{k=1}^{q} r_k\big(\hat{z}_k(l\Delta), y_c^{(i,j)}, Tl\Delta\big),\ p_{ij}(0)=1, \tag{22b}$$

for $i=1,2,\ldots,N_1$ and $j=1,2,\ldots,N_2$, with $l=0,1,\ldots,N-1$.

Third, we discretize the control input $u(\cdot)$. For any $l=0,1,2,\ldots,N-1$, we define

$$\bar{u}_l = \big(\bar{u}_{l,1}'\ \bar{u}_{l,2}'\ \ldots\ u_{l,q}'\big)', \tag{23a}$$

where $\bar{u}_{l,k}\in\mathbb{R}^{N_u}$ is the control input for the k-th patroller at scaled time $l\Delta$, $k=1,2,\ldots,q$. Here and below we use bar notation to indicate discretized quantities. Also, let

$$\bar{u} = \big(\bar{u}_0', \bar{u}_1', \ldots, \bar{u}_{N-1}'\big)', \tag{23b}$$

and for any $k=1,2,\ldots,q$ let

$$\bar{u}_{\cdot,k} = \big(\bar{u}_{0,k}', \bar{u}_{1,k}', \ldots, \bar{u}_{N-1,k}'\big)'. \tag{23c}$$

To ensure norm-preservation between the infinite-dimensional input $u(\cdot)$ and the discretized input $\bar{u}$, we scale $\bar{u}$ with the time-discretization level and let $u_k(l\Delta) = \sqrt{N}\bar{u}_{l,k}$ for all $l=0,1,\ldots,N-1$ and $k=1,2,\ldots,q$; see pp. 722-723 in [12].

Finally, let $\bar{z}_{l,q}$ be the k-th patroller's approximate state at time step l when using both the discretized dynamics (22a) and the discretized input (23b). That is, for any for $k=1,2,\ldots,q$ and for $l=0,1,\ldots,N-1$, let

$$\bar{z}_{l+1,k} - \bar{z}_{l,k} = \Delta T\,\tilde{f}(\bar{z}_{l,k}, \sqrt{N}\bar{u}_{l,k}), \bar{z}_{0,k} = \xi_k. \tag{24a}$$

Similarly, let $\bar{p}_{l,ij}$ be the approximate probability that no patroller has detected the intruder up to time step l, given that the intruder is located in the discretized area represented by $y_c^{(i,j)}$. Then we see that $\bar{p}_{l,ij}$ satisfies the difference equation,

$$\bar{p}_{l+1,ij} - \bar{p}_{l,ij} = -\Delta T\, \bar{p}_{l,ij} \sum_{k=1}^{q} r_k\big(\hat{\bar{z}}_{l,k}, y_c^{(i,j)}, Tl\Delta\big), \qquad p_{ij}(0) = 1, \quad (24b)$$

for $i = 1, 2, \ldots, N_1$ and $j = 1, 2, \ldots, N_2$, with $l = 0, 1, \ldots, N-1$. Here $\hat{\bar{z}}_{l,k}$ denotes the first two components of $\bar{z}_{l,k}$.

We emphasize that $\bar{z}_{l,k}$ depends on $T, \bar{u}_{\cdot,k}$, and ξ_k by writing $\bar{z}_{l,k}(T, \bar{u}_{\cdot,k}, \xi_k)$ instead of $\bar{z}_{l,k}$. In view of (18), the approximation of $P(T, u, \xi)$, denoted by $P_{N,N_1,N_2}(T, \bar{u}, \xi)$, using the above discretization scheme takes the form

$$P_{N,N_1,N_2}(T, \bar{u}, \xi) = \sum_{i=1}^{N_1} \sum_{j=1}^{N_2} \bar{p}_{N,ij} \phi\big(y_c^{(i,j)}\big) \Delta_1 \Delta_2. \quad (25)$$

Hence, for any positive integers N, N_1, and N_2, the time-and-space discretization of **OPPP** takes the form

$$\begin{aligned}
\mathbf{OPPP}(N, N_1, N_2): \quad & \max\{1 - P_{N,N_1,N_2}(T, \bar{u}, \xi)\} && (26a)\\
\text{s.t. } & \bar{z}_{N,k}(T, \bar{u}_{\cdot,k}, \xi_k) = g(\xi_k), k = 1, 2, \ldots, q, && (26b)\\
& \bar{z}_{l,k}(T, \bar{u}_{\cdot,k}, \xi_k) \le z_{l,k}^{\max}(T), k = 1, 2, \ldots, q, l = 0, 1, \ldots, N, && (26c)\\
& \bar{z}_{l,k}(T, \bar{u}_{\cdot,k}, \xi_k) \ge z_{l,k}^{\min}(T), k = 1, 2, \ldots, q, l = 0, 1, \ldots, N, && (26d)\\
& T \in [T^{\min}, T^{\max}], && (26e)\\
& \bar{u}_{l,k} \in \big[u_k^{\min}/\sqrt{N}, u_k^{\max}/\sqrt{N}\big], k = 1, 2, \ldots, q, l = 0, 1, \ldots, N-1, && (26f)\\
& \xi \in \mathbf{X}, && (26g)
\end{aligned}$$

where $z_{l,k}^{\max}(T) = z_k^{\max}(l\Delta; T)$ and $z_{l,k}^{\min}(T) = z_k^{\min}(l\Delta; T)$. The constraints (26b)–(26d) and (26f) are discretized versions of the corresponding constraints in **OPPP**.

The problem $\mathbf{OPPP}(N, N_1, N_2)$ has a large number of decision variables, and the dimension of the underlying augmented discrete dynamics (24a) and (24b) is also large. Specifically, the dimension of the dynamics is $n_x q + N_1 N_2$ as seen from (24a) and (24b), and the number of decision variables in $\mathbf{OPPP}(N, N_1, N_2)$ is $N n_u q + n_x q + 1$, i.e., number of control inputs plus number of initial conditions and plus the one-dimensional patrol duration.

To solve $\mathbf{OPPP}(N, N_1, N_2)$, one can use collocation methods [2], which treat the control and the state as independent variables. Although, in this case, the gradient computations become relatively simple, the resulting nonlinear programming problem has a large number of variables and a large number of nonlinear (collocation) equality constraints, representing the dynamics. Since the dimension of the augmented discrete dynamics is, normally, quite large, using collocation methods would result in serious numerical difficulties unless a solver specialized in dealing with a large number of sparse collocation constraints is used. The pseudospectral method, also known as the orthogonal collocation method [6] may reduce the size of N, and therefore the number of variables and discretized constraints. However, it has only been validated for the solution of optimal control problems with continuous optimal controls, but our patrolling problem results in discontinuous optimal controls. Hence we prefer to use the method presented in Chapter 4 of [12], which regards only control inputs, initial conditions, and end time as decision variables. Numerical results based on this approach are presented in the next section.

5. NUMERICAL RESULTS

In the following numerical examples, we assume that the k-th patroller's absolute state $x_k(t) = (x_k^1(t)\, x_k^2(t)\, x_k^3(t))' \in \mathbb{R}^3$, i.e., $n_x = 3$, where $(x_k^1(t), x_k^2(t))$ represent the absolute location of the k-th patroller, as before, and x_k^3 represents its heading. We assume that all patrollers move at constant speed v. The control input for the k-th patroller $u_k \in \mathbb{R}$ is its yaw rate, i.e., $n_u = 1$. This leads to kinematic equations in (12) defined by

$$f(x_k(t), u_k(t)) = \begin{bmatrix} v \cos x_k^3(t) \\ v \sin x_k^3(t) \\ u_k(t) \end{bmatrix}, \quad (27)$$

$k = 1, 2, \ldots, q$. This planar kinematic model describes underwater vehicles that navigate at a constant depth and a constant forward speed with variable yaw rate. In [7], a

similar model was suggested for use with underwater vehicles, but they regarded the vehicle's yaw rate as a function of vehicle's forward speed and steering angle.

After transformation to the relative state form in (13a), we obtain that

$$\tilde{f}(z_k(s), u_k(s)) = \begin{bmatrix} v\cos z_k^3(s) \\ v\sin z_k^3(s) + v_I \\ u_k(s) \end{bmatrix}. \tag{28a}$$

In **OPPP**, for every patroller $k = 1, 2, \ldots, q$, we let end-state constraint

$$g(\xi_k) = \left(\xi_k^1, \xi_k^2 + v_I, \xi_k^3 + 2n\pi\right)' \tag{28b}$$

for some $n = 0, 1, 2, \ldots$. This ensure that the absolute location and heading of the patroller at time T is the same as at time 0. The integer n is a variable that determines the number of 360-degree rotations that are required during a patrol and hence, as we will shortly see, it largely determines the shape of the trajectory. Since we cannot deal with mixed integer programming, we will resolve the problem for $n = 0, 1, 2, \ldots$. In fact, it soon becomes apparent that one can expect the largest probability of detection for the values $n = 0, 1$.

We set the state-trajectory constraints $z_k^{\min}(s;T) = (0, v_I sT - \gamma, -\infty)'$ and $z_k^{\max}(s;T) = (L, v_I sT + \gamma, \infty)'$ for $k = 1, 2, \ldots, q$, where $\gamma > 0$ is a constant that we vary below. We note the state-trajectory constraints imply that $z_k^1(s) \in [0, L]$, i.e., the patrollers stay within the channel and $z_k^2(s) \in [-\gamma + v_I sT, \gamma + v_I sT]$, i.e., $x_k^2(t) \in [-\gamma, \gamma]$. Hence, the last constraint limits how much the patrollers can travel up and down the channel. The control input limits $u_k^{\max} = 1$ and $u_k^{\min} = -1$ for $k = 1, 2, \ldots, q$. We let the constraint set on the initial conditions be given by $\mathbf{X} = \{\xi \in \mathbb{R}^3 | 0 \le \xi^1 \le L, \xi^2 = 0, \xi^3 \in \mathbb{R}\}$.

We set the channel width $L = 20$, where one unit of length equals 1000 yards, and the intruder speed $v_I = 3$, and the patroller speed $v = 1$. We assume that one unit of time equals 0.1 hours. Hence, the intruder and patrollers move at ~15 knots and 5 knots, respectively. Moreover, the control input limits mean that the patrollers change their headings with at most one radian per 0.1 hour. We always use $T^{\min} = 5$ and hence we do not consider patrols of shorter duration that 0.5 hours. We vary $T^{\max}$. We use the detection rate function (1) with parameters as given below that equation. Hence, the detection rate function is as in Fig. 2. If not stated otherwise, we assume that the distribution of the intruder's y^1-location is uniform, i.e., $\phi^1(y^1) = 1/L$. We set the discretization levels with $N = 128$ and $N_1 = N_1 = 32$. For the above parameter values, the augmented discrete dynamics are of dimension 1027, 1030, and 1033 for one, two, and three patrollers, respectively. The number of decision variables is 132, 263, and 394 for one, two, and three patrollers, respectively.

Table 1. Summary of numerical results for a single patroller and varying number of rotations n (see (28b)), vertical range γ, and patrol-duration limit $T^{\max}$.

Case	n	γ	$T^{\max}$	T^*	P^*
1	0	$L/10$	25	24.001	0.43348
2	1	$L/10$	25	23.568	0.43300
3	2	$L/10$	25	25.000	0.43243
4	0	$L/5$	15	15.000	0.42462
5	1	$L/5$	15	15.000	0.42620

T^* and P^* are optimized patrol duration and probability of detection, respectively.

Finally, we use SNOPT version 6.2 [10] in TOMLAB MATLAB toolbox [5] as our nonlinear programming solver, running on a desktop computer with two AMD Opertron 2.2 GHz processors with 8 GB RAM, running Linux 2.6.28. We use SNOPT default parameters.

Next we describe the results of several numerical studies involving one, two, and three patrollers. As the numerical results depend on the geometry of the channel, characteristics of the patrollers, and their sensors, the obtained trajectories are only illustrations of output from the proposed methodology.

5.1. One Patroller

Table 1 provides numerical results for a single patroller, i.e., $q = 1$, for several values of the number of rotations n (see (28b)), vertical trajectory constraint γ, and maximum patrol duration $T^{\max}$. In cases 1-3, $\gamma = L/10 = 2$, i.e., the patroller cannot move vertically (in Fig. 1) more than two units above or below its starting point. Moreover, in cases 1-3, the patrol duration is limited to $T^{\max} = 25$. Case 1 requires the patroller to return to the same heading at the end of the patrol (i.e., no rotation is allowed and $n = 0$ in (28b)) forcing the optimized trajectory to have a "bow-tie" shape, as displayed in Fig. 3 (solid line). Since **OPPP**(N, N_1, N_2) may be nonconvex, we cannot guarantee that the control input that generates this trajectory or those reported below are globally optimal. However, the optimized control inputs and corresponding trajectories satisfy the default stopping criterion of SNOPT and hence are close to a stationary solution of **OPPP**(N, N_1, N_2). Figure 3 also displays the initial trajectory before optimization (dotted line). The arrows in Fig. 3 and all other figures indicate the direction of travel for the patroller. Large white and black triangles denote initial positions and headings before and after optimization, respectively. Since the patroller's sensor range is roughly 5 units (see Fig. 2), the optimized trajectory is stretched out so that the sensor effectively reaches both sides of the channel. The initial trajectory has probability of detection 0.42145 and length of patrol 15,

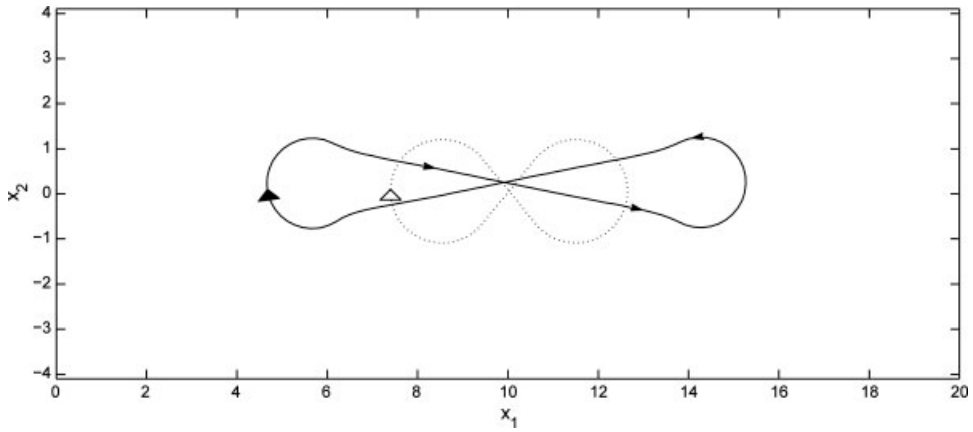

Figure 3. Case 1: Initial trajectory (dotted line) and optimized trajectory (solid line) of a single patroller with no rotation [$n = 0$ in (28b)]. The arrows indicate direction of travel for the patroller. The white triangle denotes initial position and heading before the optimization, and the black triangle denotes the one after optimization.

while the corresponding optimized numbers are 0.43348 and 24.001 as listed under T^* and P^* in Table 1.

Figure 4 illustrates the "coverage" of the channel in Case 1. Specifically, it displays the probability of no detection $\bar{p}_{N,ij}\phi(y_c^{(i,j)})$ at various relative locations (i, j). In the left portion of Fig. 4, giving the probabilities for the initial trajectory, large areas are not "covered" and thereby allowing the intruder a high chance of success. For the optimized trajectory (right portion), the situation is somewhat improved. Though, visually this may be difficult to identify.

Case 2 in Table 1 is identical to Case 1 but requires a 360-degree heading change at the end of one patrolling period (i.e., $n = 1$). Hence, the patroller must return to a heading shifted 360 degrees from the initial heading, which excludes a "bow-tie" type trajectory, but is compatible with a "racetrack" type trajectory. Figure 5 shows the corresponding initial trajectory (dotted line, probability of detection is 0.42587) and optimized trajectory (solid line, probability of detection is 0.43300). We note that the optimized probability of detection is slightly worse for $n = 1$ than for $n = 0$, 0.43348 versus 0.43300.

Case 3 in Table 1 is identical to Case 1 but requires two rotations (i.e., $n = 2$), which rules out both "bow-tie" and "racetrack" type trajectories. In this case, the initial heading must be shifted by 720 degrees and hence the patroller makes two loops as shown in Fig. 6. The probability of detection is again slightly worse than for $n = 0$ and $n = 1$. Since the probability of detection seems to decrease as the number of rotations increases, we will, as a heuristic, restrict ourselves to the problems with $n = 0$ and 1.

In Cases 1 and 2, the patrol-duration limit $T^{\max}$ is not active. In Cases 4 and 5 this limit is reduced to 15 and also the vertical movement restriction γ is relaxed to $L/5 = 4$. We see from Table 1 that these changes impose a restriction on the patroller and the probability of detection worsens. Figures 7 and 8 show the resulting trajectories. We see that the worsened probability of detection is caused by the fact that the shorter patrol duration prevents the patroller from reaching the sides of the channel.

We also consider a situation (Case 6) where the distribution of the intruder's y^1-location is not uniform. Suppose that $\phi^1(y^1) = 2y^1/L$. Hence, we assume that the intruder is more likely to travel down the channel near the right side than the left side in Fig. 1. Figure 9 shows the optimized trajectory for this case with no rotation required ($n = 0$), $\gamma = L/10$, and

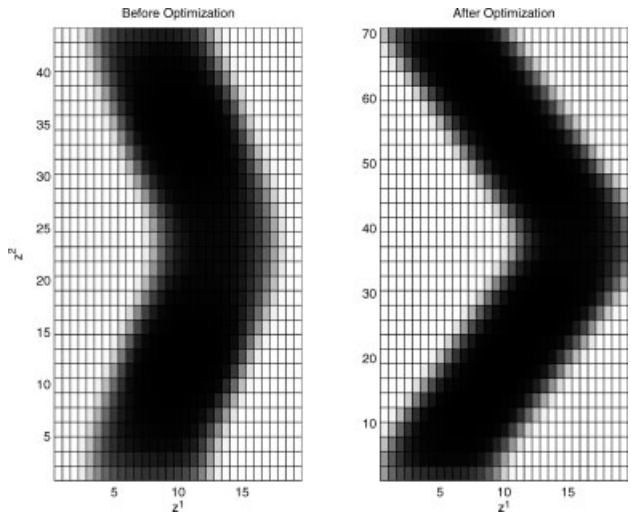

Figure 4. Case 1: Coverage of channel before (left) and after (right) optimization in relative locations as measured by the probability of no detection $\bar{p}_{N,ij}\phi(y_c^{(i,j)})$; see (25). Shades of gray represent different probability levels with black being 0 and white 1.

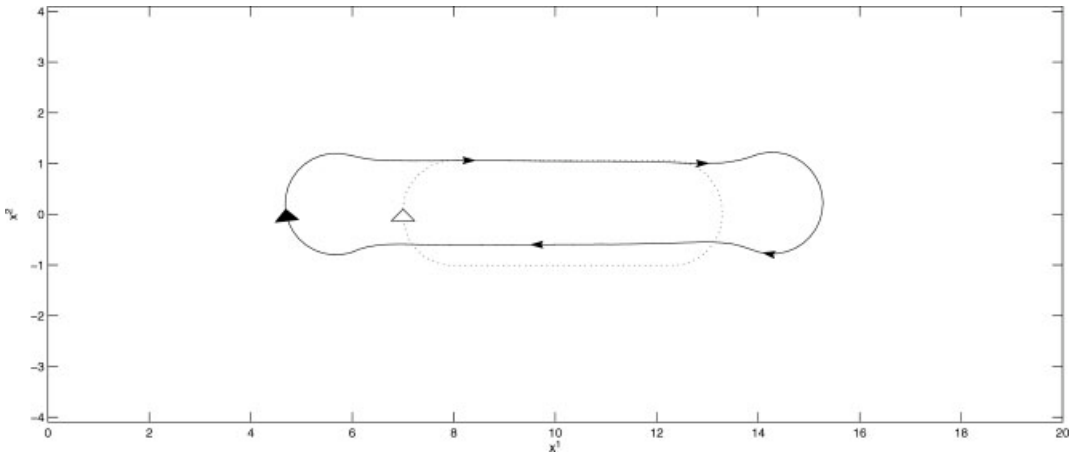

Figure 5. Case 2: Initial trajectory (dotted line) and optimized trajectory (solid line) of a single patroller with 360-degree rotation [$n = 1$ in (28b)].

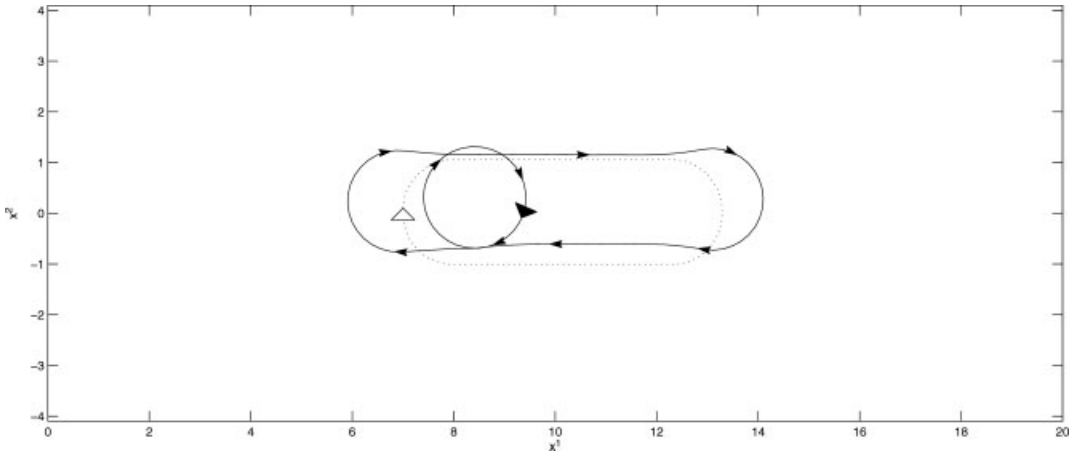

Figure 6. Case 3: Initial trajectory (dotted line) and optimized trajectory (solid line) of a single patroller with 720-degree rotation [$n = 2$ in (28b)].

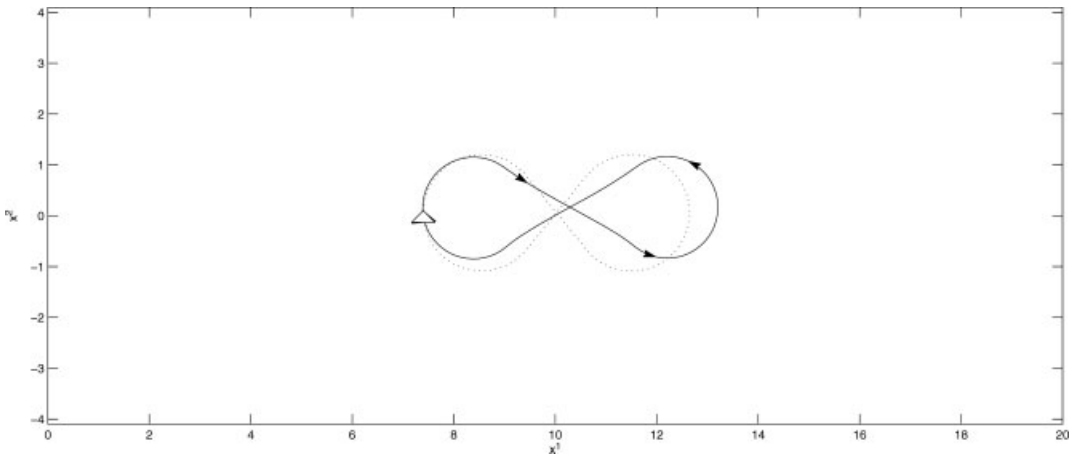

Figure 7. Case 4: Initial trajectory (dotted line) and optimized trajectory (solid line) of a single patroller with no rotation [$n = 0$ in (28b)] and patrol duration restriction.

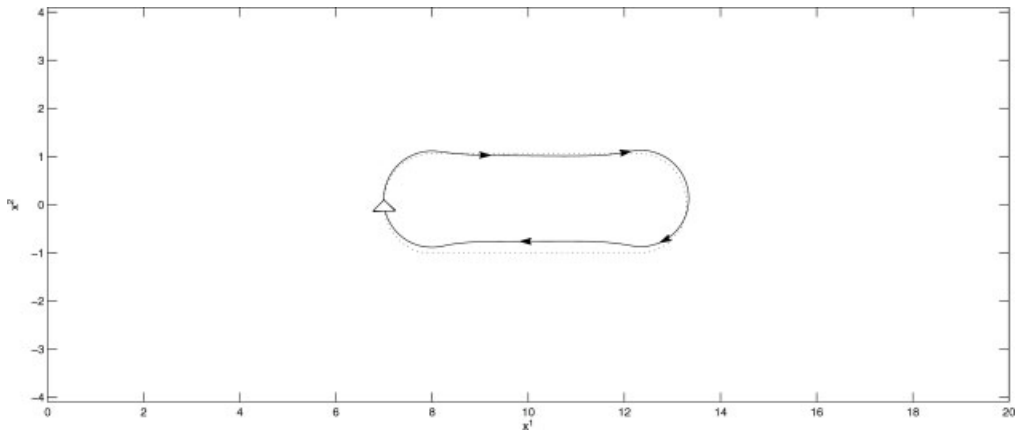

Figure 8. Case 5: Initial trajectory (dotted line) and optimized trajectory (solid line) of a single patroller with 360-degree rotation [$n = 1$ in (28b)] and patrol duration restriction.

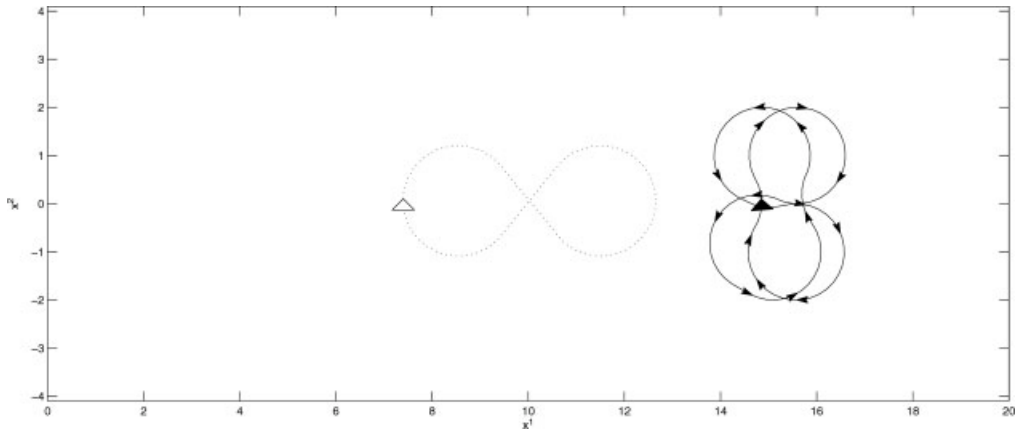

Figure 9. Case 6: Initial trajectory (dotted line) and optimized trajectory (solid line) of a single patroller with no rotation [$n = 0$ in (28b)] and right-leaning triangular intruder-location distribution.

$T^{\max} = 25$. We see that in this case the patroller prefers a "double figure eight" trajectory close to the right side of the channel. The optimized trajectory has duration 25.000 and significantly improves the probability of detection to 0.61374 from the initial probability of detection of 0.42449.

We return to the situation with a uniform intruder distribution and consider the effect of variable intruder speed. Table 2 presents Cases 7-12 involving different intruder speeds and numbers of rotation. We assume that detection rate is as above, even though a slower intruder may be quieter and therefore harder to detect under certain circumstance. In all of these cases $\gamma = L/10$ and $T^{\max} = 25$. Rows two and three of Table 2 restate the results for Cases 1 and 2 from Table 1, in which the intruder speed $v_I = 3$, for ease of comparison. Rows four and five give results for $v_I = 2$. Naturally, as the intruder speed reduces, the probability of detection increases, while the shapes of trajectories remain qualitatively similar (Fig. 10). This effect is further observed for the Cases 9 and 10 ($v_I = 1$) and for Cases 11 and 12 ($v_I = 0.5$). We note that in all cases the constraint of no rotation ($n = 0$) results in better probability of detection than the requirement

Table 2. Summary of numerical results for a single patroller, varying intruder speed v_I, and number of rotations n (see (28b)), with $\gamma = L/10$ and $T^{\max} = 25$.

Case	v_I	n	T^*	P^*
1	3	0	24.001	0.43348
2		1	23.568	0.43300
7	2	0	23.578	0.49725
8		1	23.178	0.49514
9	1	0	24.177	0.65767
10		1	24.434	0.64077
11	0.5	0	25.000	0.88680
12		1	25.000	0.86413

T^* and P^* are optimized values of patrol duration and probability of detection, respectively.

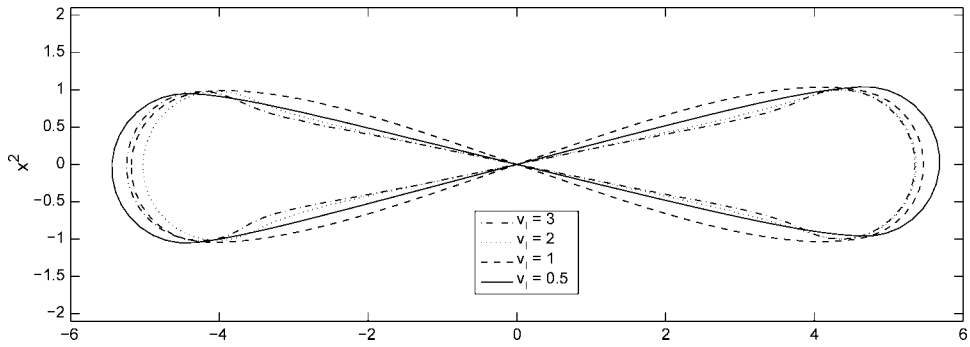

Figure 10. Zoomed-in solution trajectories with varying v_I and $n = 0$ [see (28b)]. For ease of comparison, the trajectories are slightly translated so that the crossing points of the trajectories are at the origin.

of a 360-degree rotation ($n = 1$). These results are qualitatively different from the "idealized" results obtained in [15], Chapter 9, which do not account for turn radius constraints of the patroller. There we see that a "back-and-forth" trajectory similar to the one in Fig. 5 ($n = 1$), but with infinitely sharper turns, is better than a "bow-tie" trajectory similar to that in Fig. 3 ($n = 0$) whenever v/v_I is less than 1.8. Since Cases 1, 2, 7-10 involve smaller v/v_I ratios, the "idealized" results would lead to the conclusion that a "back-and-forth" trajectory would be best. However, our numerical results show that the bow-tie trajectory ($n = 0$) is better when the patroller is constrained by its turn radius.

5.2. Two Patrollers

Next we consider two patrollers, i.e., $q = 2$, and five additional cases as summarized in Table 3. In all of these cases the patrol-duration limit $T^{\max} = 25$. Rows two and three of Table 3 give the optimized patrol duration and probability of detection for no rotation ($n = 0$) and 360-degree rotation ($n = 1$), respectively, using $\gamma = L/10$. Figures 11 and 12 give the corresponding trajectories. We see again that no rotation (Case 13) results in better probability of detection. Figure 11 shows that the optimized trajectories are similar to "figure eights," even though the initial trajectories are similar to the infinity symbol. This effect is caused by the narrowness of the channel. The two patrollers obtain better probability of detection and less overlap in their "coverage" by moving along

Table 3. Summary of numerical results for two patrollers, varying number of rotations n (see (28b)), and vertical range γ.

Case	n	γ	T^*	P^*
13	0	L/10	25.000	0.82037
14	1	L/10	11.633	0.79340
15	0,1	L/10	25.000	0.81234
16	0	L/5	25.000	0.82354
17	1	L/5	25.000	0.81594

T^* and P^* are the optimized patrol duration and probability of detection, respectively. For all cases in the table the patrol-duration limit $T^{\max} = 25$.

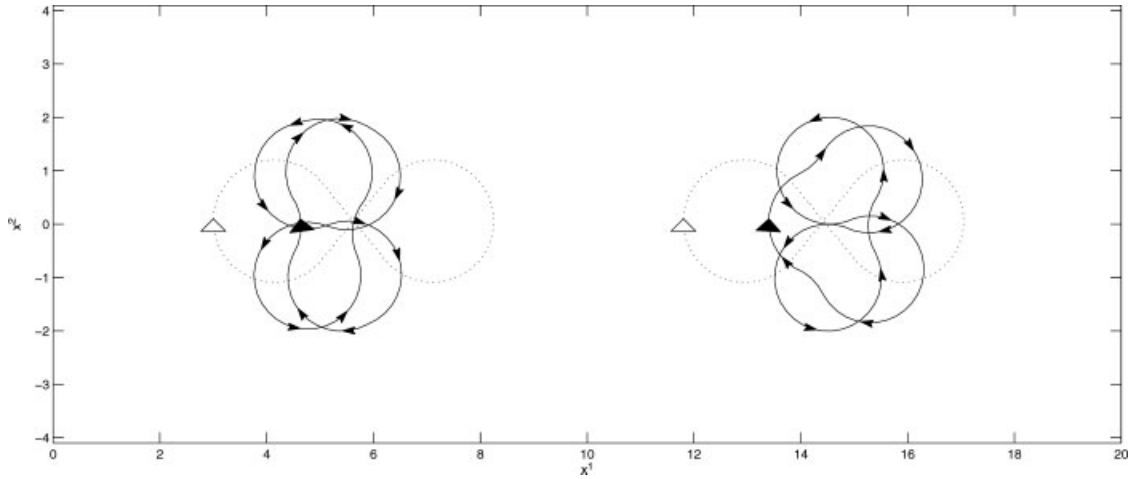

Figure 11. Case 13: Initial trajectories (dotted line) and optimized trajectories (solid line) of two patrollers with no rotation [$n = 0$ in (28b)].

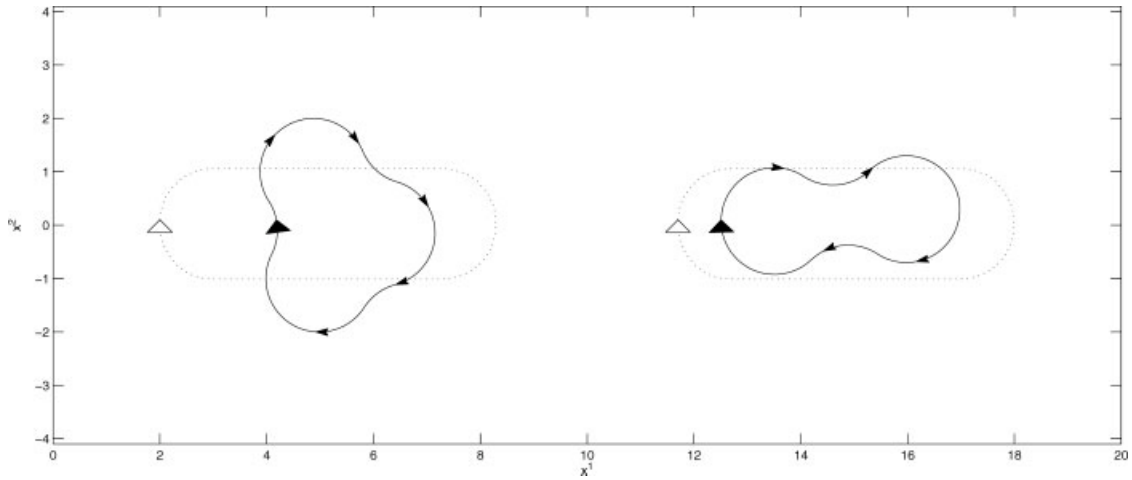

Figure 12. Case 14: Initial trajectories (dotted line) and optimized trajectories (solid line) of two patrollers with 360-degree rotation [$n = 1$ in (28b)].

the channel instead of across. The probability of detection for the initial trajectory is 0.78003 and improves to 0.82037 after optimization.

We observe that the trajectories in Fig. 11 are different for the two patrollers, which may be counterintuitive as the distribution of the intruder's y^1-location is uniform. Additional calculations show that the trajectories in Fig. 11 yield a larger probability of detection (0.82037) than patrol plans consisting of identical but translated trajectories for both patrollers. If the right-most patroller mimics the left-most patroller in Fig. 11, but on the right side of the channel, then the probability of detection deteriorates to 0.81630. If the left-most patroller mimics the right-most patroller, then the probability of detection deteriorates to 0.81472. The probabilities deteriorate further when the patrollers carry out identical but mirror-imaged trajectories. These results provide new insight that is not easily obtained using the idealized calculations of [15], Chapter 9.

The optimized trajectories of Case 14 with the constraint of one rotation (i.e., $n = 1$) (see Fig. 12) yield a probability of detection of 0.79340, which is worse than in Case 13 (i.e., $n = 0$). Figure 13 illustrates the coverage of the channel in this case. We note that the initial trajectory (left portion of Fig. 13) leaves some locations poorly covered. The optimized trajectory is somewhat better in that regard as shown by the right portion of Fig. 13.

We also examined the configuration with one patroller constrained to no rotation ($n = 0$) and the other one to a 360-degree rotation ($n = 1$), and denote it by Case 15; see Fig. 14. However, the resulting probability of detection (0.81234) is worse than in Case 13.

Cases 16 and 17 in Table 3 show results similar to those for Cases 13 and 14, but for $\gamma = L/5$. With this relaxation of the vertical movement constraint for the patrollers, we obtain slightly better probability of detection. The relaxation allows for more complicated patrol trajectories as shown in Figs. 15 and 16. We see that the patrollers stagger vertically their trajectories to avoid overlap and therefore increase the probability of detection. While not easily seen from Figs. 15 and 16, the patrollers also synchronize their progress along their trajectories so that when one patroller moves to the left, say, then the other tends to move to the left also to fill the gap between the patrollers. Figures 17 and 18 illustrate this effect by showing the coverage map and the relative locations of the patrollers during $t \in [0, T]$ for Case 17, respectively. Such insight about the coordination between multiple patrollers cannot be reached through single-patroller analysis. The initial trajectories in Case 17 result in a probability

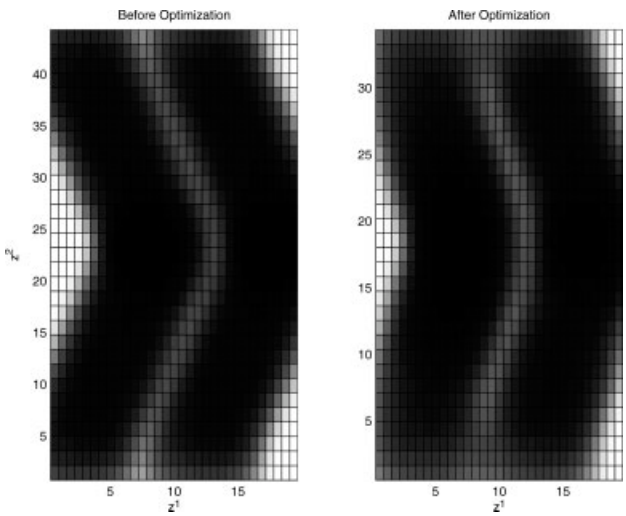

Figure 13. Case 14: Coverage of channel before (left) and after (right) optimization similar to Fig. 4.

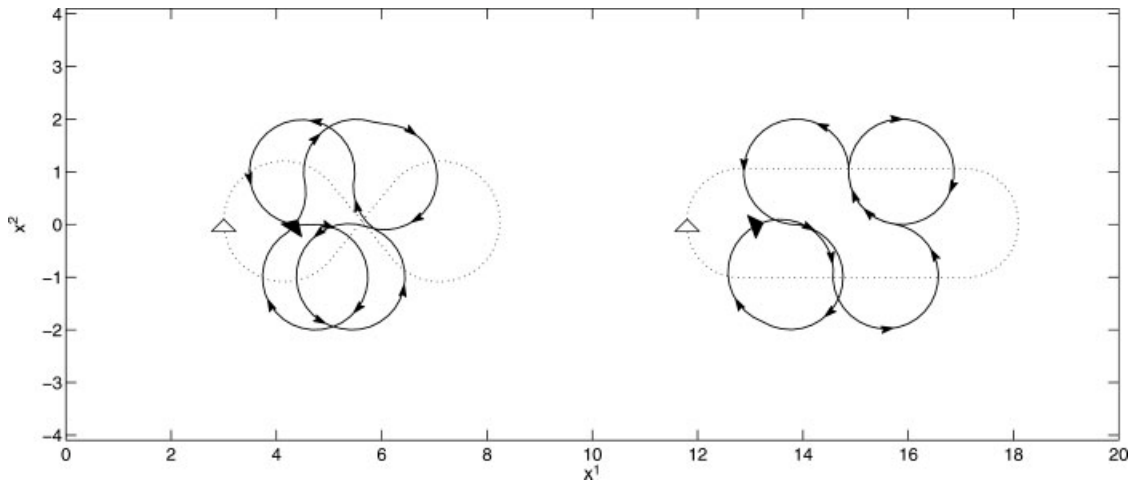

Figure 14. Case 15: Initial trajectories (dotted line) and optimized trajectories (solid line) of two patrollers with no rotation ($n = 0$) and one rotation ($n = 1$) in (28b).

of detection of 0.77806, which is improved to 0.81594 after optimization.

5.3. Three Patrollers

Finally, we consider three patrollers briefly, for the single case of $T^{\max} = 25$, $\gamma = L/10$, and no rotation constraint ($n = 0$). The optimized probability of detection is 0.94086, improved from 0.90335 for the initial trajectories, and the optimized patrol duration is $T^* = 25.000$. Figures 19 and 20 display the initial and optimized trajectories in absolute locations and in terms of coverage, respectively. We see that the shape of each trajectory is quite similar to the ones in Case 13 for two patrollers; see Fig. 11. We note that for two and three patrollers the optimized trajectories tend to become quite intricate, especially when the patrollers are tightly constrained vertically with $\gamma = L/10$ and no rotation is required ($n = 0$). This effect is caused by the fact that multiple patrollers make it suboptimal for each patroller to search across the whole channel. This would have caused substantial overlap between the patrollers and a lower probability of detection. Hence, each patroller is effectively confined to a smaller area of operations. Even in the smaller area, the patrollers tend to prefer longer patrol durations and the constraint $T \leq T^{\max}$ is often active. Longer patrol durations are usually preferable as the constraint that the patroller's relative final state must match its relative initial state (possibly with a rotational shift) imposes a restriction on the patroller and the longer duration allows more "free" movement between those "boundary conditions."

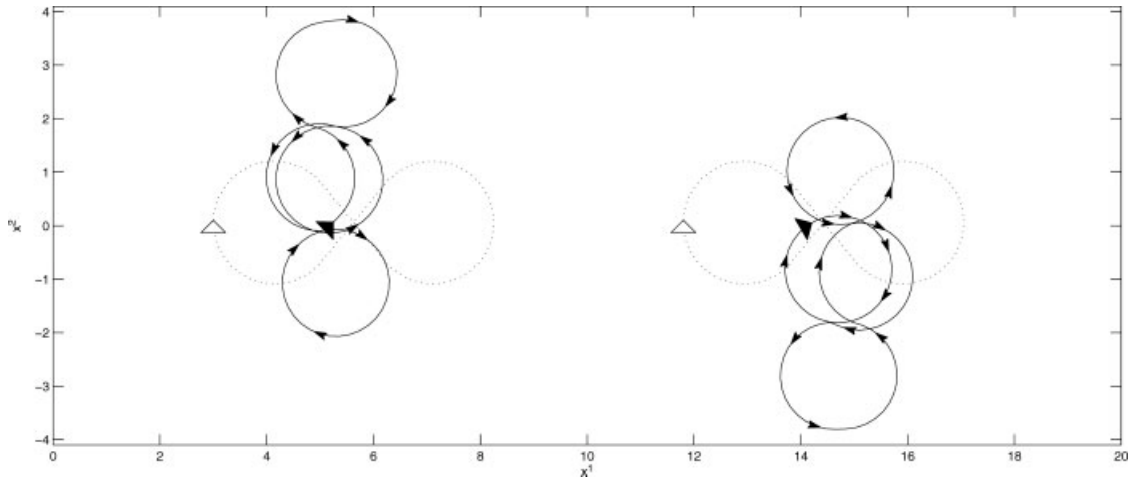

Figure 15. Case 16: Initial trajectories (dotted line) and optimized trajectories (solid line) of two patrollers with no rotation [$n = 0$ in (28b)] and relaxed vertical trajectory constraint.

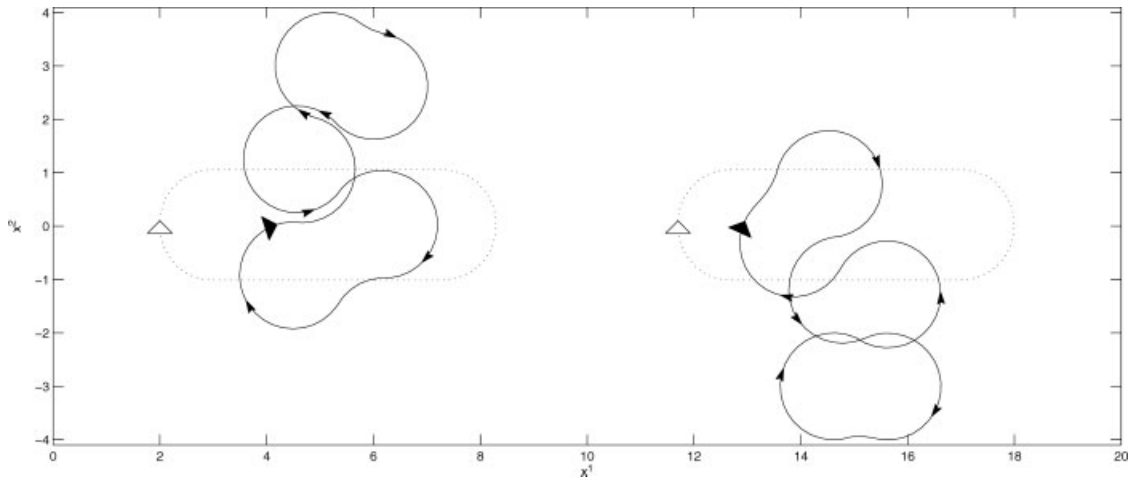

Figure 16. Case 17: Initial trajectories (dotted line) and optimized trajectories (solid line) of two patrollers with 360-degree rotation [$n = 1$ in (28b)] and relaxed vertical trajectory constraint.

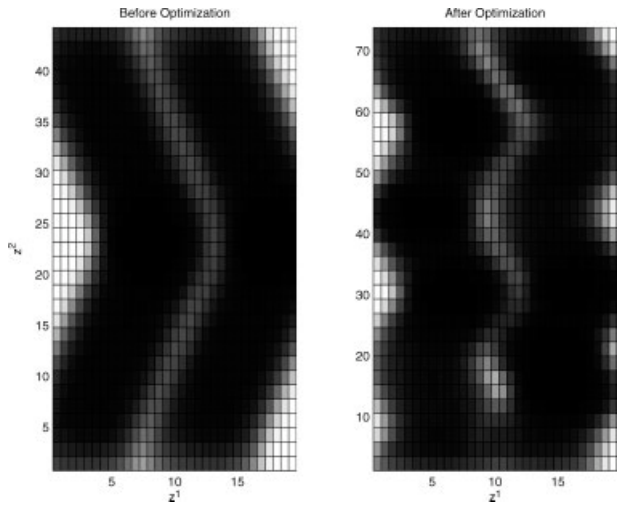

Figure 17. Case 17: Coverage of channel before (left) and after (right) optimization similar to Fig. 4.

6. CONCLUSIONS

We formulated the channel patrol problem for multiple patrollers subject to turn-rate constraints as an optimal control problem. In this problem, the patrollers aim to maximize the probability of detecting an intruder that travels straight down a channel with constant speed. Using discretization of time and space, we obtained a large-scale nonlinear programming approximation of that problem which we solved to obtain an approximately stationary solution and a corresponding optimized trajectory for each patroller. In numerical tests specifically tailored to one, two, and three underwater patrollers, an underwater intruder, different trajectory constraints, and several intruder speeds, we found that simple "back-and-forth" trajectories across the channel are inferior to more complicated, optimized trajectories. For a single patroller, the optimized trajectories tend to have the shape of a bow tie for a variable range of intruder speeds. The optimized trajectory changes shape to a "double figure eight" when the intruder is known to bias its route to one side of the channel. For two patrollers, the optimized trajectories also take the shape of "double figure eights," which may be staggered when the trajectory constraints allow sufficient movement along the channel. For three patrollers, the optimized trajectories again resemble "double figure eights." The optimized probability of detecting an intruder at 15 knots in a channel of width 20,000 yards using three patrollers at 5 knots with an imperfect sensor of range ∼5,000 yards is 0.94. That probability is reduced to 0.82 and 0.43 for two and one patrollers, respectively.

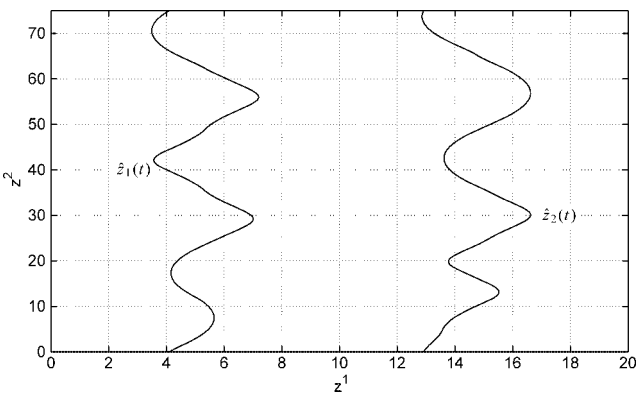

Figure 18. Case 17: Relative locations $\hat{z}_1(t) = (z_1^1(t), z_1^2(t))$ and $\hat{z}_2(t) = (z_2^1(t), z_2^2(t))$ for two patrollers with absolute location given in Fig. 16.

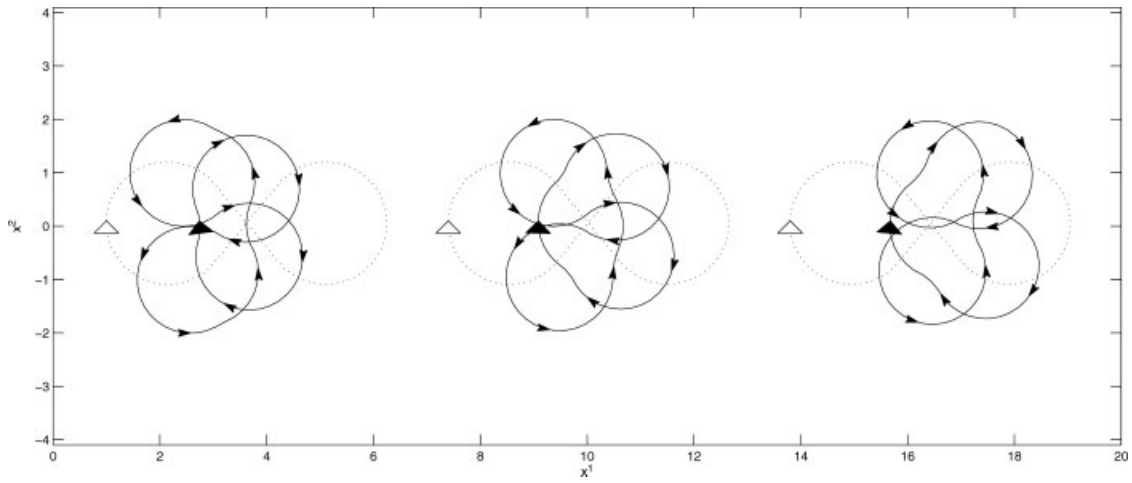

Figure 19. Case 18: Initial trajectories (dotted line) and optimized trajectories (solid line) of three patrollers with no rotation [$n = 0$ in (28b)] constraint.

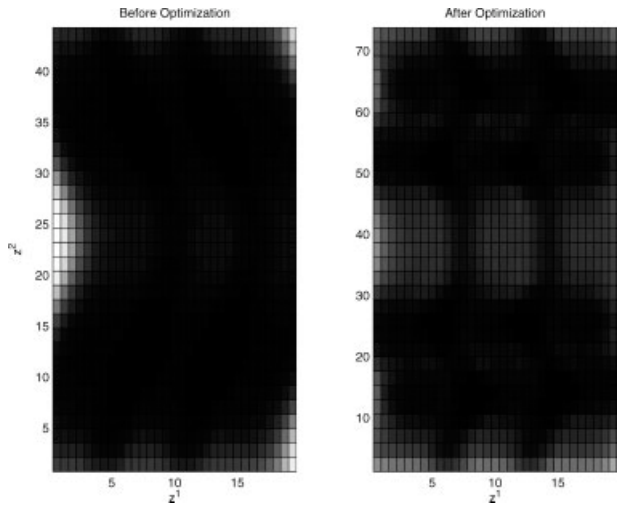

Figure 20. Case 18: Coverage of channel before (left) and after (right) optimization similar to Fig. 4.

The results of this study provide new insight, not easily obtained using geometric calculations, into efficient patrol trajectory design for multiple patrollers in a narrow channel where interaction between the patrollers is unavoidable due to their limited turn rate. The insight comes at a substantial computational cost as the large-scale nonlinear programming approximations may require many days to solve using standard hardware and software due to expensive function and gradient evaluations as well as poor conditioning. We believe it is possible to obtain significant reductions in computing times, but defer such efforts to future studies.

APPENDIX

In this appendix we describe a three-dimensional extension of the model and discretization scheme presented in Sections 2–4.

Now we let $\hat{x}_k(t) \triangleq (x_k^1(t), x_k^2(t), x_k^3(t)) \in \mathbb{R}^3$ and $\hat{z}_k(t) \triangleq (z_k^1(t), z_k^2(t), z_k^3(t)) \in \mathbb{R}^3$ be the absolute and relative position, respectively, of the k-th patroller at time t, $k = 1, 2, \ldots, q$, where

$$\begin{aligned} z_k^1(t) &= x_k^1(t) \\ z_k^2(t) &= x_k^2(t) + v_I t \\ z_k^3(t) &= x_k^3(t). \end{aligned} \tag{A1}$$

Suppose that the channel has width L_1 and depth L_3. Then, it suffices to consider relative intruder position $y \in A(T) \triangleq [0, L_1] \times [0, v_I T] \times [0, L_3]$ for patrols of duration T time units. The probability that no patroller detects the intruder during $[0, T]$ then takes the same form as (11), but with $\hat{z}_k(t) \in \mathbb{R}^3$, $y \in \mathbb{R}^3$, $\phi(y) = \phi^1(y^1)\phi^3(y^3)/(v_I T)$, with $\phi^3(y^3)$ being the probability density function of the intruder's depth and $r_k(\cdot, \cdot, \cdot)$ being the obvious extension of the detection rate function to three dimensions. The problem formulation **OPPP** remains identical after the changes discussed above with an integration over the volume $A = [0, L_1] \times [0, v_I] \times [0, L_3]$ in (18).

The discretization scheme in three dimension takes the following form. We now use N_1 by N_2 by N_3 grid points defined by

$$y_{i_1}^1 = i_1 \Delta_1 \text{ and } y_{i_2}^2 = i_2 \Delta_2 \text{ and } y_{i_3}^3 = i_3 \Delta_3, \tag{A2}$$

where $\Delta_1 = L_1/N_1$, $\Delta_2 = v_I/N_2$, $\Delta_3 = L_3/N_3$, $i_j = 0, 1, \ldots, N_j$, and $j = 1, 2, 3$. We also define center points of the grid by

$$y_c^{(i_1,i_2,i_3)} = \begin{bmatrix} y_{i_1}^1 - \Delta_1/2 \\ y_{i_2}^2 - \Delta_2/2 \\ y_{i_3}^3 - \Delta_3/2 \end{bmatrix}, \tag{A3}$$

for $i_j = 1, 2, \ldots, N_j$ and $j = 1, 2, 3$.

Let $p_{i_1 i_2 i_3}(s) \triangleq p(y_c^{(i_1,i_2,i_3)}, s)$. Then, for the center points of this grid, (17) becomes

$$\frac{dp_{i_1 i_2 i_3}(s)}{ds} = -T p_{i_1 i_2 i_3}(s) \sum_{k=1}^{q} r_k\big(\hat{z}_k(s), y_c^{(i_1,i_2,i_3)}, Ts\big), p_{i_1 i_2 i_3}(0) = 1. \tag{A4}$$

The discretization of the dynamics in time takes the form (22a) and

$$p_{i_1 i_2 i_3}((l+1)\Delta) - p_{i_1 i_2 i_3}(l\Delta) = -\Delta T p_{i_1 i_2 i_3}(l\Delta) \sum_{k=1}^{q} r_k\big(\hat{z}_k(l\Delta), y_c^{(i_1,i_2,i_3)}, Tl\Delta\big), p_{i_1 i_2 i_3}(0) = 1, \quad \text{(A5)}$$

for $i_j = 1, 2, \ldots, N_j$, $j = 1, 2, 3$, and $l = 0, 1, \ldots, N-1$. The discretized control input is identical to the 2-dimensional case. The patroller's approximate state when using both the discretized dynamics and the discretized input is as in (24a). The approximate probability that no patroller has detected the intruder up to time step l, given that the intruder is located in the discretized area represented by $y_c^{(i_1,i_2,i_3)}$ is given by $\bar{p}_{l,i_1 i_2 i_3}$, which satisfies the difference equation

$$\bar{p}_{l+1,i_1 i_2 i_3} - \bar{p}_{l,i_1 i_2 i_3} = -\Delta T \bar{p}_{l,i_1 i_2 i_3} \sum_{k=1}^{q} r_k\big(\hat{\bar{z}}_{l,k}, y_c^{(i_1 i_2 i_3)}, Tl\Delta\big), p_{i_1 i_2 i_3}(0) = 1, \quad \text{(A6)}$$

for $i_j = 1, 2, \ldots, N_j$, $j = 1, 2, 3$, and $l = 0, 1, \ldots, N-1$. Here $\hat{\bar{z}}_{l,k}$ denotes the first three components of $\bar{z}_{l,k}$. The approximate probability (25) generalizes to

$$P_{N,N_1,N_2,N_3}(T, \bar{u}, \xi) = \sum_{i_1=1}^{N_1} \sum_{i_2=1}^{N_2} \sum_{i_3=1}^{N_3} \bar{p}_{N,i_1 i_2 i_3} \phi\big(y_c^{(i_1,i_2,i_3)}\big) \Delta_1 \Delta_2 \Delta_3. \quad \text{(A7)}$$

Hence, the time-and-space discretization of **OPPP** in three dimensions takes the same form as **OPPP**(N, N_1, N_2), but with $P_{N,N_1,N_2}(T, \bar{u}, \xi)$ replaced by $P_{N,N_1,N_2,N_3}(T, \bar{u}, \xi)$.

ACKNOWLEDGMENTS

HC, EP, and SS were partially supported by ONR MURI "Computational Methods for Collaborative Motion" (CoMotion), and ARO MURI "Scalable SWARMS of Autonomous Robots and Mobile Sensors" (SWARMS). JOR is supported by AFOSR Young Investigator grant F1ATA08337G003 and ONR Science of Autonomy Program.

REFERENCES

[1] S.J. Benkoski, M.G. Monticino, and J.R. Weisinger, A survey of the search theory literature, Nav Res Logist 38 (1991), 469–494.
[2] J.T. Betts, Survey of numerical methods for trajectory optimization, AIAA J Guid Contr Dynam 21 (1998), 193–207.
[3] S.D. Bopardikar, F. Bullo, and J.P. Hespanha, A cooperative Homicidal Chauffeur game, Automatica 45 (2009), 1771–1777.
[4] O. Hellman, On the optimal search of a randomly moving target, SIAM J Appl Math 22 (1972), 545–552.
[5] K. Holmström, A.O. Göran, and M.M. Edvall, User's Guide for TOMLAB, Tomlab Optimization Inc., Vasteras, Sweden, 2006.
[6] G.T. Huntington, Advancement and analysis of a Gauss pseudospectral transcription for optimal control problems, PhD thesis, Massachusetts Institute of Technology, 2007.
[7] G. Indiveri, Kinematic time-invariant control of a 2d nonholonomic vehicle, IEEE Conference on Decision and Control, Phoenix, AZ, 1999, pp. 2112–2117.
[8] B.O. Koopman, Search and screening, Operations Evaluation Group Report 56, Center for Naval Analysis, Alexandria, Virginia, 1946.
[9] T.G. McGee and J.K. Hedrick, Guaranteed strategies to search for mobile evaders in the plane, In: Proceedings of the 2006 American Controls Conference, Minneapolis, MN, 2006, pp. 2819–2824.
[10] W. Murray, P.E. Gill, and M.A. Saunders, SNOPT: an SQP algorithm for large-scale constrained optimization, SIAM J Optim 12 (2002), 979–1006.
[11] A. Ohsumi, Optimal search for a Markovian target, Nav Res Logist 38 (1991), 531–554.
[12] E. Polak, Optimization: Algorithms and consistent approximations, Vol. 124 of Applied Mathematical Sciences, Springer, Berlin, 1997.
[13] United States of America The Department of Navy, The navy unmanned undersea vehicle (UUV) master plan, 2004.
[14] R. Vidal, O. Shakernia, H.J. Kim, D.H. Shim, and S. Sastry, Probabilistic pursuit-evasion games: Theory, implementation, and experimental evaluation, IEEE Trans Robot Autom 18 (2002), 662–669.
[15] D.H. Wagner, W.C. Mylander, and T.J. Sanders, Naval operations analysis, Naval Institute Press, Annapolis, MD, 1999.
[16] A.R. Washburn, Search and detection, 4th ed., INFORMS, Linthicum, Maryland, 2002.
[17] A.R. Washburn, On patrolling a channel, Nav Res Logist 29 (1982), 609–615.